Amplitude-encoding FWI using different bases

He. Liu, Daniel. Trad, Kristopher. Innanen

ABSTRACT

A super-shot or blended data strategy has been used in marine and land seismic surveys to reduce acquisition costs by reducing the time spent on the field. Full waveform inversion (FWI) has been used to estimate high-resolution subsurface velocity models. However, it suffers from expensive computational costs for matching the synthetic and the observed data. To reduce the costs of both data acquisition and processing, FWI using blended data has been recognized as very promising in future oil exploration. In this work, we use an amplitude-encoding strategy with different bases to accelerate the FWI process and compare their performance. The synthetic examples show that amplitude-encoding FWI using different bases as encoding functions can mitigate the crosstalk noise very well, providing good estimations of velocity models and convergence rate for both acoustic and elastic media. To further improve the calculation efficiency, we also adopt the dynamic encoding concept and reduce the number of super-shots every a few iterations. Since the encoding functions are not changed during the iterations, we can directly simulate the super-shots without the blending stage. From the updated velocity model comparison, we can see that the inversion results by dynamic encoding are almost identical to those by static encoding with further reduced calculation effort.

INTRODUCTION

FWI is a high-resolution seismic imaging technique that is based on using the entire content of seismic traces for extracting physical parameters of the medium sampled by seismic waves (Virieux et al., 2017). The classical time-domain FWI was originally proposed by Tarantola (1984) to invert the velocity model by minimizing the l2-norm of the difference between predicted and observed data (Symes, 2008). This technique is very useful but computationally expensive.

To reduce the costs of both data acquisition and processing, a simultaneous source-firing strategy has been recognized as very promising in future oil exploration. Increasing field efficiency by recording more than one source has been explored utilizing encoded shot gathers or super-shots (Romero et al., 2000). However, once the super-shots are acquired, traditional seismic processing methods require a de-blending process for velocity model estimation and seismic migration (Florez et al., 2016).

Source-encoding strategies were first introduced into pre-stack migration in the frequency domain (Morton and Ober, 1998; Romero et al., 2000). Krebs et al. (2009) proposed to multiply the source wavelet with a random encoding sequence of +1 or -1 and then blend all the shot gathers into one super-shot. Zhan et al. (2009) proposed to compose a multi-source shot gather of a sum of single-shot gathers with random time delays. This usually requires zero-padding the input shot gathers along the time axis, which may add extra cost for the time-domain wave extrapolator and memory. Dai et al. (2012) proposed to combine these two source-encoding strategies for least-squares reverse time migration (LSRTM).

Usually, all shots are blended into several sub-super-shots that contain all the shot records. Hu et al. (2016) proposed an efficient amplitude encoding strategy using a cosine basis to perform LSRTM. Godwin and Sava (2013) proposed an amplitude encoding strategy using Hartley basis for wave-equation migration and compared its performance with some other source-encoding strategies. To date, source-encoding strategies have been used to accelerate RTM, LSRTM and FWI process (Krebs et al., 2009; Dai et al., 2012; Godwin and Sava, 2013; Pan, 2017). Instead of modifying the phase or zero-padding the input shot gathers, the implementation of the amplitude encoding method is based on weighting the amplitude of the shot gathers. Therefore, it can be conveniently incorporated into the time-domain wave propagator. What is also different is that one super shot contains all the shot gathers.

In this work, we present amplitude encoding acoustic and elastic FWI using different bases and compare the inversion results. We also adopt the dynamic encoding concept and change the number of super-shots every a few iterations to further reduce the calculation effort.

AMPLITUDE-ENCODING FWI IN TIME DOMAIN

In the case of constant density, the acoustic wave equation is described by

$$\frac{1}{v^2(\mathbf{x})} \frac{\partial^2 p(\mathbf{x}, t; \mathbf{x}_s)}{\partial t^2} - \nabla^2 p(\mathbf{x}, t; \mathbf{x}_s) = f_s(\mathbf{x}, t; \mathbf{x}_s) \tag{1}$$

where $f_s(x, t; x_s) = f(t') \delta(x - x_s) \delta(t - t')$.

In the classical first-order velocity-stress formulation (e.g., Collino and Tsogka (2001)), the elastic wave equation can be written as

$$\begin{aligned} \rho \partial_t \mathbf{v} &= \nabla \cdot \sigma \\ \partial_t \sigma &= \mathbf{c} : \nabla \mathbf{v} \end{aligned} \tag{2}$$

where $\mathbf{v}$ is the velocity vector and σ is the second-order stress tensor, $\mathbf{c}$ is the full elastic tensor with up to 21 independent coefficients and ρ is the density.

Let's first focus on the acoustic case, according to equation 1, the data misfit $\Delta p = p_{cal} - p_{obs}$ can be defined by the differences at the receiver positions between the recorded seismic data p_{obs} and the forward modeled seismic data $p_{cal} = f(m)$ for each source-receiver pair of the seismic survey. In the acoustic velocity inversion, $f(\cdot)$ indicates the forward modeling function, whereas m corresponds to the velocity model to be inverted. The goal of FWI is to match the data misfit by iteratively updating the velocity model. We also define the data misfit function as the objective function taking the least-squares norm of the misfit vector Δp, which is given by

$$\begin{aligned} E(\mathbf{m}) &= \frac{1}{2} \Delta \mathbf{p}^\dagger \Delta \mathbf{p} = \frac{1}{2} \|\mathbf{p}_{\text{cal}} - \mathbf{p}_{\text{obs}}\|^2 \\ &= \frac{1}{2} \sum_{r=1}^{ng} \sum_{s=1}^{ns} \int_0^{t_{\max}} \mathrm{d}t \, |p_{\text{cal}}(\mathbf{x}_r, t; \mathbf{x}_s) - p_{\text{obs}}(\mathbf{x}_r, t; \mathbf{x}_s)|^2 \end{aligned} \tag{3}$$

where ns and ng are the number of sources and receivers and $\dagger$ denotes the adjoint operator (conjugate transpose).

In encoding FWI, shot gathers are transformed into super shot gathers by the encoding matrix, which is defined as

$$\mathbf{B} = \begin{bmatrix} b^{1,1} & b^{2,1} & . & b^{N_{ig},1} \\ b^{1,2} & b^{2,2} & . & b^{N_{sig},2} \\ . & . & . & . \\ b^{1,N_{sup}} & b^{2,N_{sup}} & . & b^{N_{sig} \cdot N_{sup}} \end{bmatrix} \tag{4}$$

where N_{sup} is the number of the super-shots and N_{sig} is the number of the individual shots ($N_{sup} < N_{sig}$). The N_{sig} synthetic data and observed data are blended into N_{sup} blended data by

$$\begin{aligned} \mathbf{p}_{\text{cal}}^{\text{sup}} &= \mathbf{B}\mathbf{p}_{\text{cal}} \\ \mathbf{p}_{\text{obs}}^{\text{sup}} &= \mathbf{B}\mathbf{p}_{\text{obs}} \end{aligned} \tag{5}$$

The ratio between N_{sig} and N_{sup} is the factor by which the computational cost is reduced. Since usually N_{sup} is much smaller than N_{sig}, the encoding FWI would achieve much better efficiency due to the reduction of data dimension. Then the encoding objective function is given by:

$$\begin{aligned} E(\mathbf{m}) &= \frac{1}{2}\Delta\mathbf{p}^{\dagger}\Delta\mathbf{p} = \frac{1}{2}\left\|\mathbf{p}_{\text{cal}} - \mathbf{p}_{\text{obs}}\right\|^2 \\ &= \frac{1}{2}\left(p_{\text{cal}} - p_{\text{obs}}\right)\mathbf{B}^{\text{T}}\mathbf{B}\left(p_{\text{cal}} - p_{\text{obs}}\right) \end{aligned} \tag{6}$$

The matrix $\mathbf{B}^T\mathbf{B}$ is referred to as the crosstalk matrix, and when it's equal to the identity matrix, the encoding objective function is equal to the traditional objective function. FWI using blended data would produce the same results as in conventional FWI cases. Therefore, to make the inversion result from the encoding FWI comparable with that from the conventional FWI, the designed encoding crosstalk matrix should be a good approximation of the identity matrix.

In this work, we use different bases as the encoding functions to design the amplitude encoding matrices.

The Hartley encoding matrix is defined as (Tsitsas, 2010):

$$b_{m,n} = \cos\left(\frac{2\pi mn}{n_{\text{sig}}}\right) + \sin\left(\frac{2\pi mn}{n_{\text{sig}}}\right) \tag{7}$$

The discrete form of the cosine basis is (Hu et al., 2016):

$$b_{m,n} = \sqrt{\frac{2}{n_{\text{sig}}}}\cos\left(\frac{\pi}{n_{\text{sig}}}\frac{(2m\%n_{\text{sig}}+1)(2n+1)}{4}\right) \tag{8}$$

The sine encoding matrix is defined as (Tsitsas, 2010):

$$b_{m,n} = \sqrt{\frac{2}{n_{\text{sig}}}} \sin\left(\frac{\left(m + \frac{1}{2}\right)\left(n + \frac{1}{2}\right)\pi}{n_{\text{sig}}}\right) \tag{9}$$

Also, we noticed that the random polarity encoding strategy (Krebs et al., 2009) works in a very similar way. It also applies different weights to the shot records or source wavelets to compose super-shots, except that the weights are only + 1 or -1. In addition, it composes all the individual shots into only one super-shot, and changes the encoding sequence at each iteration. In this work, we use it in a different way, we don't change the encoding sequence at each iteration, but also use it as a basis and establish a encoding matrix, and then compose multiple super-shots. Given enough number of individual shots and super-shots, the crosstalk matrix for this basis will also be close to an identity matrix. The random polarity basis can be expressed as:

$$b_{m,n} = 1 \text{ or } -1 \tag{10}$$

In equation 6 to 10, the parameters are defined in the same way, $m = 1,\ldots, N_{sig}$ is the shot-index, $n = 1,\ldots, N_{sup}$ is the super-shot index, and n_{sig} is the periodization index, which we set to be half of N_{sig}.

NUMERICAL RESULTS FOR ACOUSTIC FWI

Marmousi model

In this section, we use a Marmousi model with a distance of 9216 m and a depth of 3008 m on a grid of 16 meters discretized in a grid of 576 by 188 grid points, which is shown in Fig 1a. On top of the Marmousi model is a water layer with the thickness of 320 m, the acoustic velocity is set to 1500 m/s. which makes the whole model size 576 by 208 grid points. We get the initial model shown in Fig 1b by smoothing the original Marmousi model, but the top layer remains not smoothed.
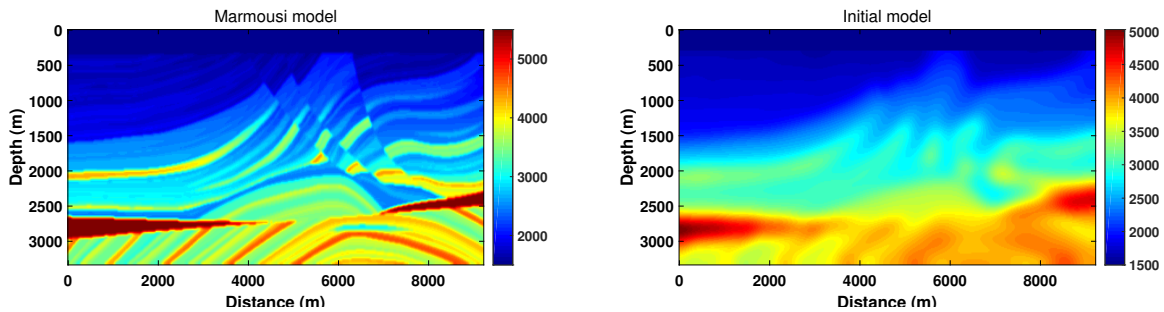

FIG. 1. (a) The original Marmousi is down sampled along depth and lateral direction. The shots are generated according to the Marmousi model. (b) The initial model of FWI for Marmousi model, which is obtained by smoothing the original model.

In this work, we generate all synthetic shot gathers by solving the acoustic wave equations in time domain for all 140 sources, which are evenly distributed near the surface of

original Marmousi model with a spatial interval of 64 m (4 grid points). We deploy 576 receivers right beneath the sources with a spatial interval of 16 m (1 grid point). The Ricker wavelet sources are fired with a central frequency of 4 Hz. We record the seismic waveforms for 4.2 s with an time step of 1.5 ms. For conventional FWI, all the sources are fired individually and shot gathers are recorded separately. For amplitude encoding FWI, we apply different amplitude weights to the shot gathers to compose super-shots.

In our experiments, we use Hartley, cosine, sine and random polarity as encoding functions. For comparison, we blend all the shot gathers into 7, 35 and 70 super-shots. Fig 2 and Fig 3 are the encoding matrices and corresponding crosstalk matrices. The elements of encoding matrices are the weights we apply to the individual shots and compose super-shots. The crosstalk matrices show how close they are to an identity matrix. We can see with an increasing number of blended data, more off-diagonal elements are close to zero.

FIG. 2. Amplitude encoding matrices: columns from left to right are by Hartley, cosine, sine and random polarity bases; rows from up to down are for 7, 35 and 70 super-shots, respectively.
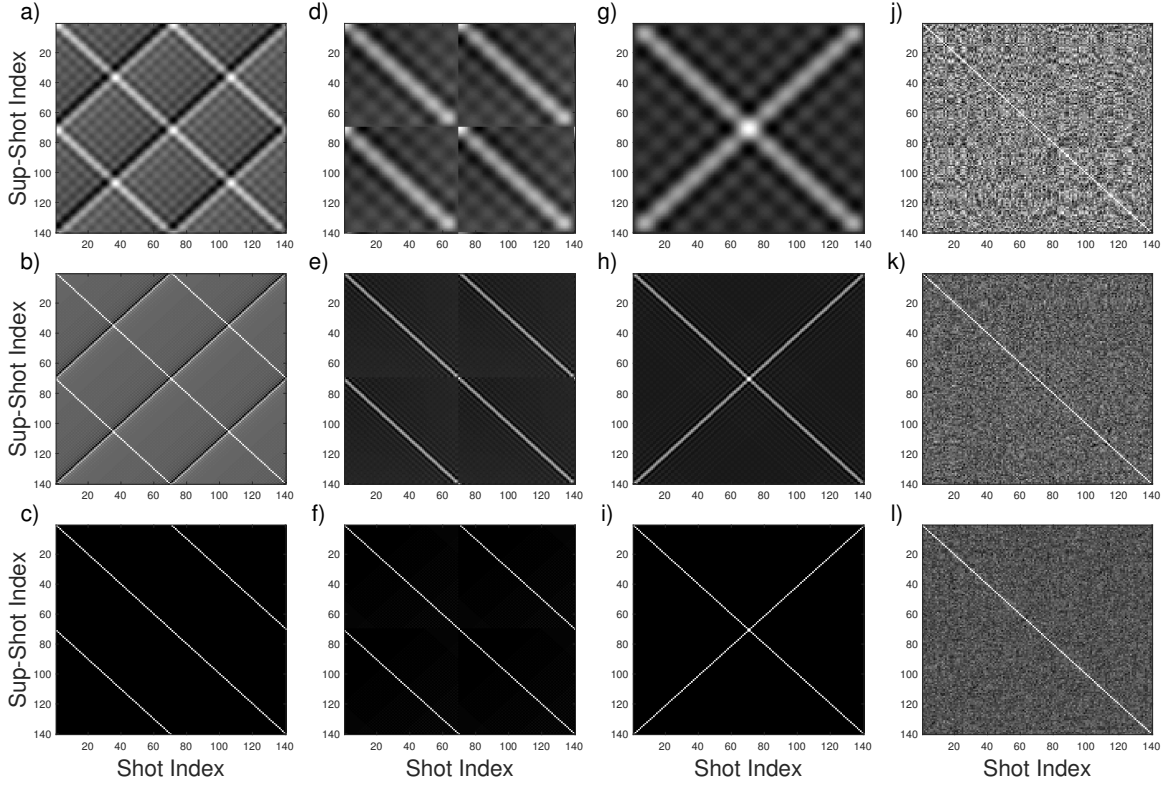
FIG. 3. crosstalk matrices: columns from left to right are by Hartley, cosine, sine and random polarity bases; rows from up to down are for 7, 35 and 70 super-shots, respectively.

In Fig 4, we present the first individual shot in the conventional case and the first super-shots in the amplitude-encoding cases using different bases. We can notice that each super-shot contains all the individual shots and information of the whole model.
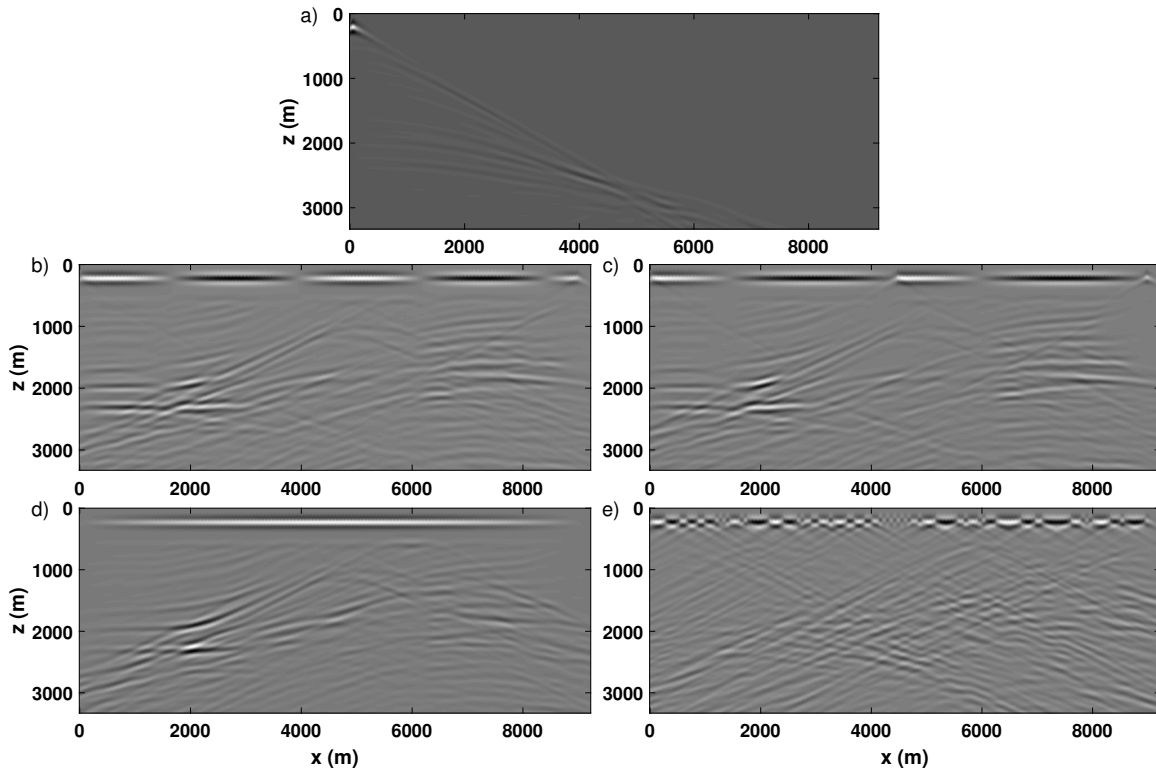
FIG. 4. a) is the first individual shot in the conventional case; b) to e) are the first super-shot in the amplitude-encoding cases.

In this work, we run FWI using a gradient-based method (Yang et al., 2015) for 100 iterations. For comparison, we first present the inversion result using conventional FWI, which is displayed in Fig 5a. Then we perform amplitude-encoding FWI using different bases as the encoding functions. For brevity, the inversion results at the early stage using 7 and 70 super-shots are shown in Fig 5b-i. When we first take a look at the left column using 7 super-shots (see Fig 5b, d, f and h), we can notice there exists some crosstalk noise in the middle left or upper left, while with increasing number of super-shots (see results using 70 super-shots in the right column in Fig 5), the crosstalk noise can be better mitigated and the images are almost noise-free.
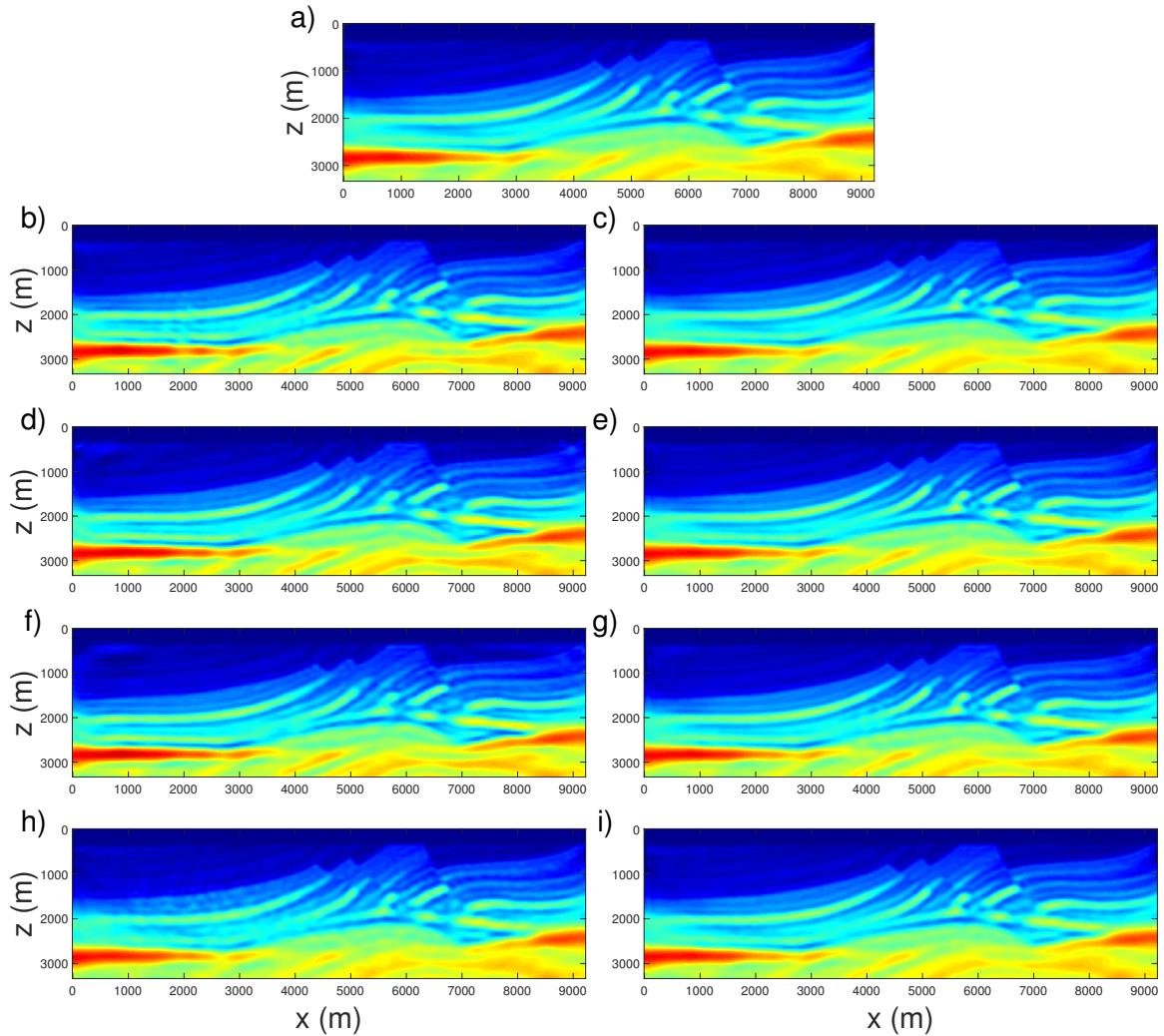
FIG. 5. The updated velocity models after 25 iterations: a) by conventional FWI; b) and c) are by Hartley basis with 7 and 70 super-shots; d) and e) are by cosine basis with 7 and 70 super-shots; f) and g) are by sine basis with 7 and 70 super-shots; h) and i) are by random polarity basis with 7 and 70 super-shots.

The inversion results after 100 iterations are shown in Fig 6. Generally, in our experiments, compared with the result by conventional FWI in Fig 6a, we can see amplitude-encoding FWI using all 4 different encoding functions would produce very good estimations of the velocity model, even with only 7 super-shots (see the left columns in Fig 5 and 6). However, to achieve better imaging quality, it still requires more super-shots to mitigate the crosstalk noise with much more extra calculation effort.
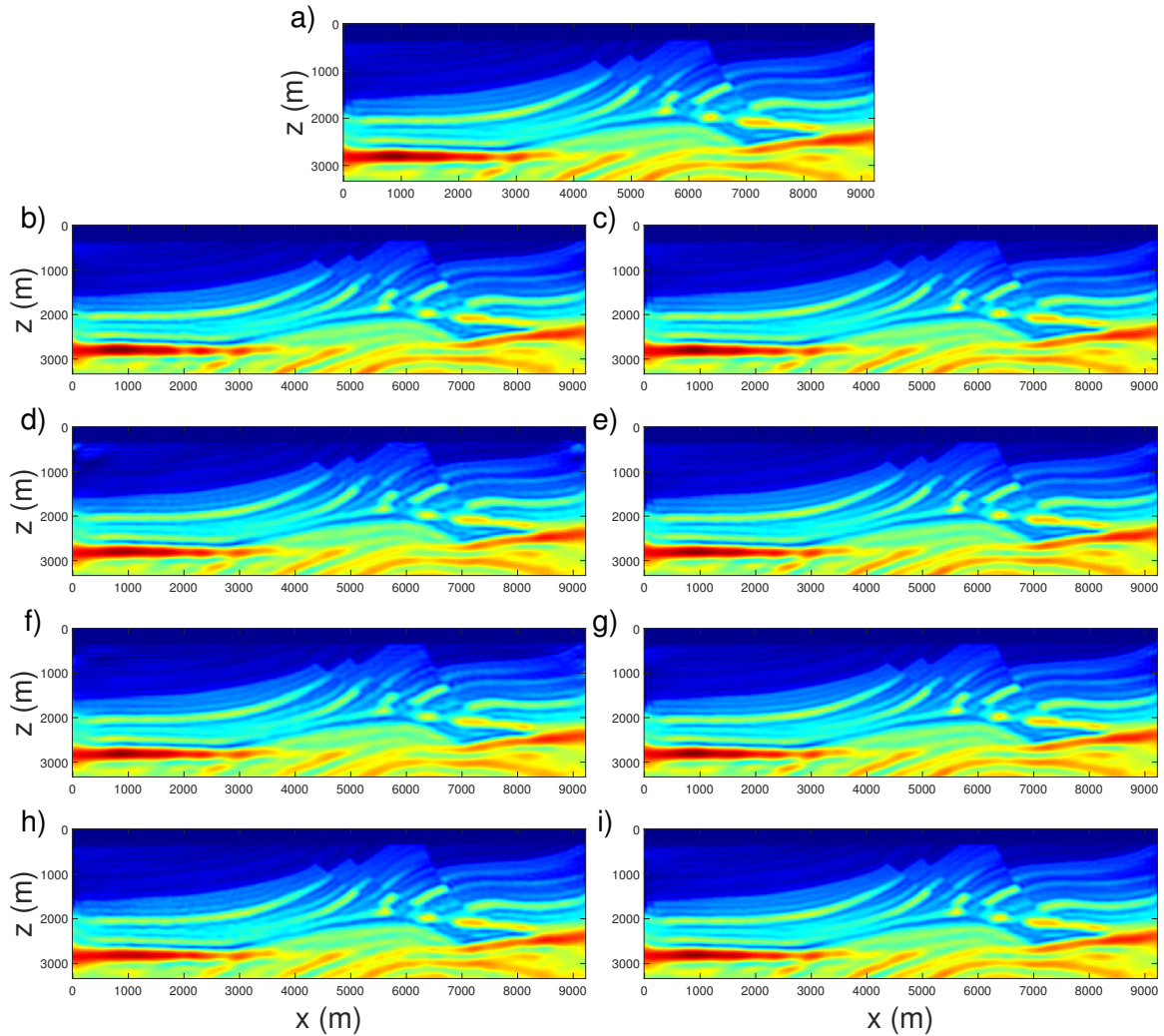
FIG. 6. The updated velocity models after 100 iterations: a) by conventional FWI; b) and c) are by Hartley basis with 7 and 70 super-shots; d) and e) are by cosine basis with 7 and 70 super-shots; f) and g) are by sine basis with 7 and 70 super-shots; h) and i) are by random polarity basis with 7 and 70 super-shots.

As shown in Fig 7, we compare the data misfits in the conventional and amplitude-encoding FWI cases using 70 super-shots encoded by different bases. Note that the maximum value of data misfit we display here is 0.2. From the comparison, we can notice that using amplitude-encoding strategy, the encoding FWI experiments show very similar convergency as in the conventional case.
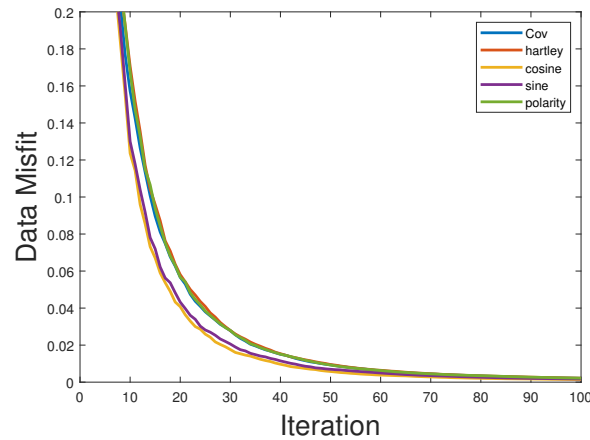
FIG. 7. Comparison of data misfit function

To obtain ideal updated velocity models with better mitigated crosstalk noise as in the 70 super-shots cases, clearly the data dimension is not reduced enough. To further improve the calculation efficiency, we adopt the dynamic encoding concept (Krebs et al., 2009). They proposed to change the encoding sequence every iteration to avoid accumulating the crosstalk noise for better imaging quality. In our case, compared to the inversion results using 70 super-shots, we can notice the crosstalk noise in the inversion results using 7 super-shots are not significant. So instead of changing the encoding functions, we dynamically reduce the number of super-shots every a few iterations to further reduce the data dimension, hoping to achieve a better compromise between imaging quality and calculation efficiency. In our test, for the first step, we still compose the individual shot gathers into 70 super-shots and run FWI for 25 iterations, then we compose the shot gathers into 35 super-shots and run FWI for another 25 iterations using the updated velocity model by the first step. Likewise, we then use 14 super-shots and 7 super-shots for 25 iterations each. So overall, we also update the velocity model 100 times.

We present the inversion results using dynamic encoding concept after 100 iterations in Fig 8. When we respectively compare them with the updated velocity models using 70 super-shots in the static-encoding cases shown in the right column of Fig 6, we can see both encoding strategies provide almost identical inversion results and using different bases make no significant difference, but the data dimension has been further reduced.
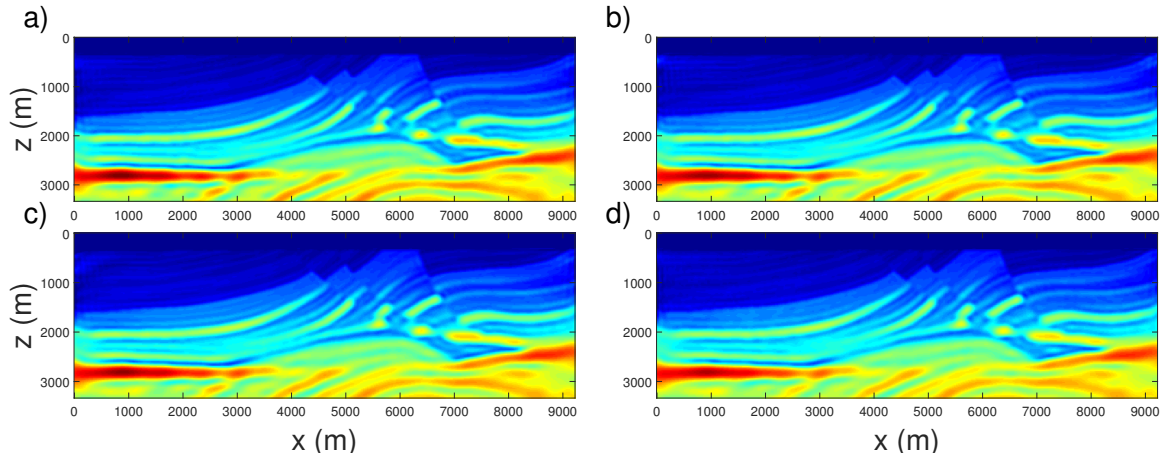
FIG. 8. Inversions results using dynamic-encoding concept by different bases: a) Hartley; b) cosine; c) sine and d) random polarity.

The data misfit and vertical profile comparisons are shown in Fig 9a and b, respectively. We can see that using dynamic encoding concept can provide a very similar convergence rate as in the static encoding cases. In addition, since the number of super-shots is changed every 25 iterations, the data misfit function curves may not be smooth. Compared to the previous static case, we can notice that using Hartley and random polarity bases, when the number of super-shot is reduced during inversion process, there might be obvious "jump" in the misfit curves. While in the cosine and sine bases cases, even the super-shot number is reduced, the curves are still very smooth. From the comparison of vertical profiles in the middle of the model, we can see the lines are almost overlapped, amplitude-encoding FWI using all different 4 bases gives very good estimations of the true velocity model.
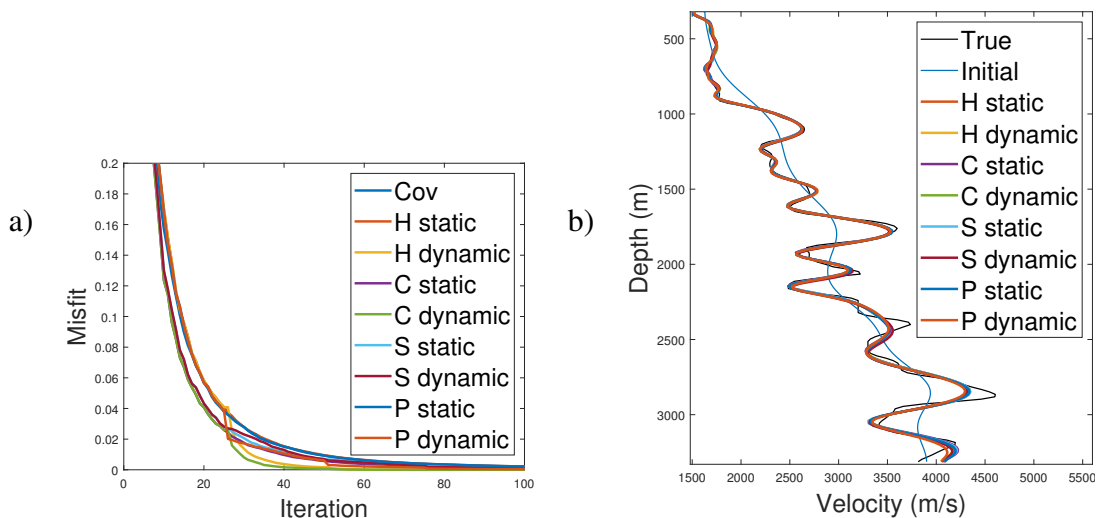

FIG. 9. a) is the comparison of vertical profiles at distance equals to 4680 m; b) is the comparison of data misfit functions versus iteration.

Foothill model

To further validate the feasibility of amplitude-encoding strategy, we also used this foothill model with a distance of 6672 m and a depth of 4000 m in a grid of 417 by 250 cells with 16 meters size each, which is shown in Fig 10a. We also get the initial model by smoothing the original Marmousi model, as shown in Fig 10b.

For this model, we generate all synthetic shot gathers for 100 sources, which are evenly distributed near the surface of true model with a spatial interval of 64 m. We deploy 417 receivers right beneath the sources with a spatial interval of 16 m. The Ricker wavelet sources are fired with a central frequency of 8 Hz. We record the seismic waveforms for 6.0 s with a time step of 1.5 ms.
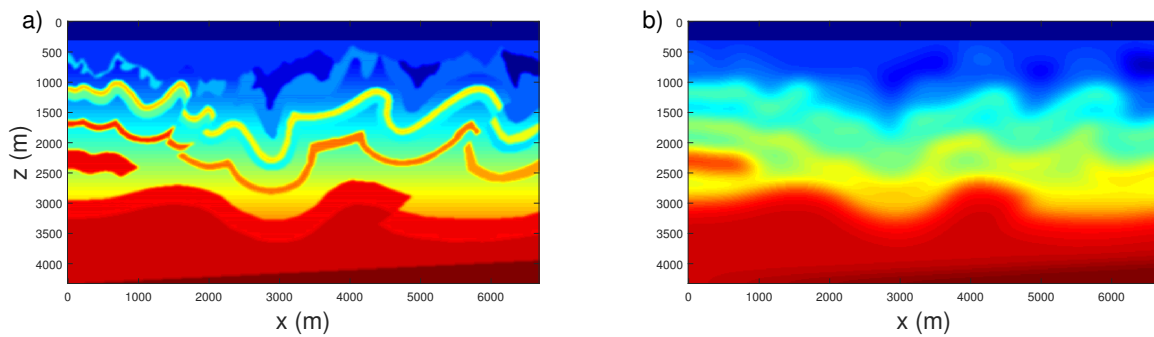

FIG. 10. a) true foothill model; b) initial model.

In this case, we compose the shot records into 50, 25, 10 and 5 super-shots, and also run FWI for 25 iterations each. For brevity, we only display the inversion results using dynamic encoding shown in Fig 11.
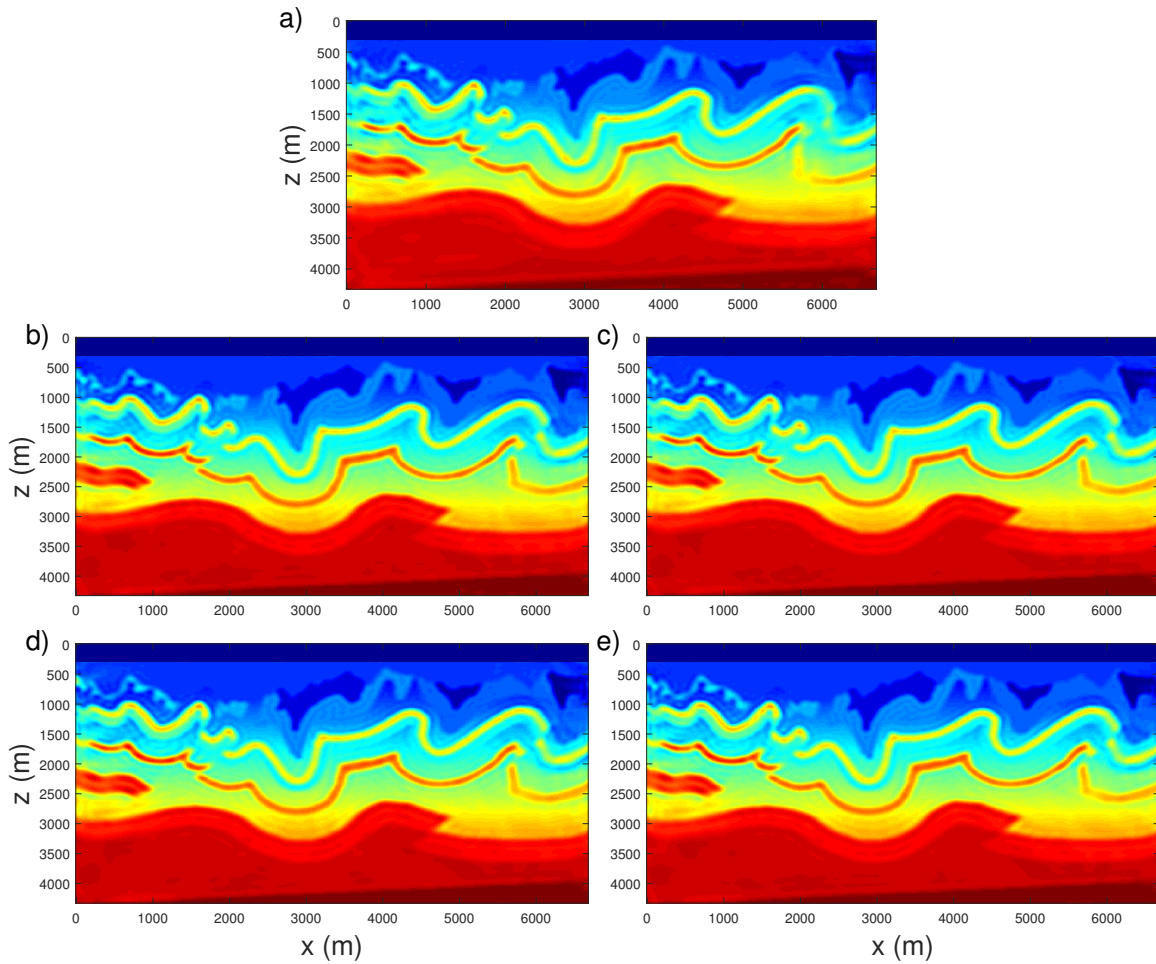
FIG. 11. Inversion results after 100 iterations: a) by conventional FWI; Inversions results using dynamic-encoding concept by: b) Hartley basis; c) cosine basis; d) sine basis; e) random polarity basis.

For this model, FWI converges really fast, data misfits reduce to 0.1 within 10 iterations as shown in Fig 12. The curves for 5 cases overlapped at the first 25 iterations. We may also see the "jump" in here, just much less obvious than the Marmousi model cases.
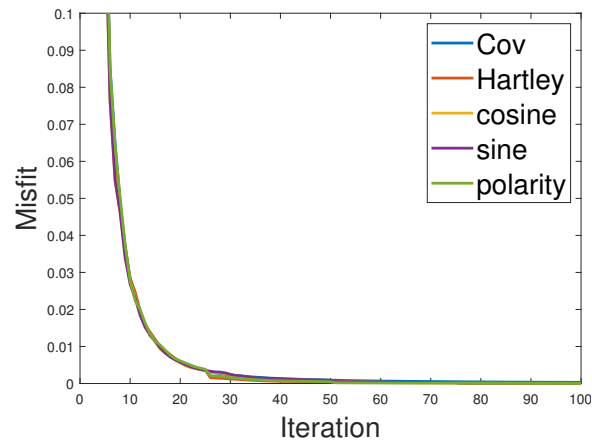

FIG. 12. Comparison of data misfit functions versus iteration using dynamic encoding concept.

NUMERICAL RESULTS FOR ELASTIC FWI

In this section, we further apply amplitude-encoding strategy into elastic FWI. In isotropic elastic media, the first-order stress-velocity wave equation can be rewritten as:

$$
\begin{aligned}
\rho \frac{\partial v_i}{\partial t} &= \frac{\partial \sigma_{ij}}{\partial x_j} + f_i \\
\frac{\partial \sigma_{ij}}{\partial t} &= \lambda \frac{\partial \theta}{\partial t} \delta_{ij} + 2\mu \frac{\partial \varepsilon_{ij}}{\partial t} \\
\frac{\partial \varepsilon_{ij}}{\partial t} &= \frac{1}{2} \left(\frac{\partial v_i}{\partial x_j} + \frac{\partial v_j}{\partial x_i} \right)^2
\end{aligned}
\tag{11}
$$

where ρ is the density, σ is the stress, v is the velocity, λ and μ are Lame coefficients, and vp and vs can be expressed by

$$
\begin{aligned}
v_p &= \sqrt{(\lambda + 2\mu)/\rho} \\
v_s &= \sqrt{\mu/\rho}
\end{aligned}
\tag{12}
$$

The objective function using l2-norm of the data misfit for elastic FWI using amplitude-encoding strategy can also be expressed as equation 6, exactly the same as in the acoustic case. So when the crosstalk matrix is a good approximation of the identity matrix, amplitude-encoding strategy should also work for elastic FWI in the same way. In this work, we use the IFOS2D software (Bohlen et al., 2016) to do the experiments.

We use a subsampled Marmousi II elastic model with a distance of 3600 m and a depth of 1100 m in a grid of 360 by 110 cells with 10 meters size each. This model consists of a 200 m thick water layer above. The true and initial models are shown in Fig 13, we only perform FWI for vp and vs in this work.
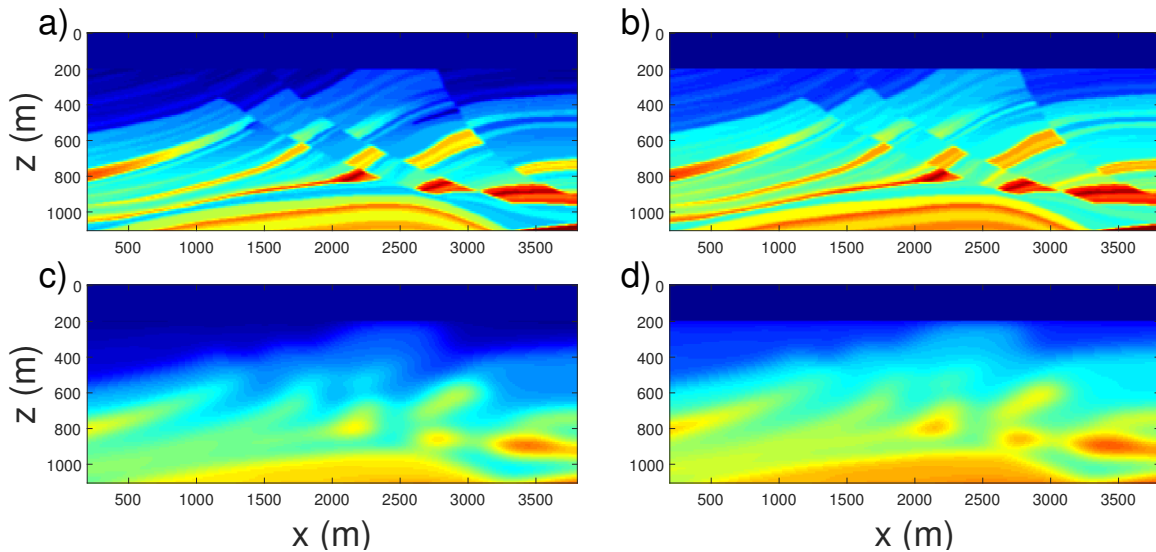

FIG. 13. Subsampled Marmousi II model: a) and b) are true vp and vs; c) and d) are initial vp and vs.

We generate synthetic shot gathers for 40 explosive sources and deploy 360 two–component receivers. The central freq is 10 hz. The sources and receivers are at depth 20 and 30 meters, respectively.

In this experiment, we compose all 40 individual shots into 20 super-shots, the encoding and crosstalk matrices are shown in Fig 14.
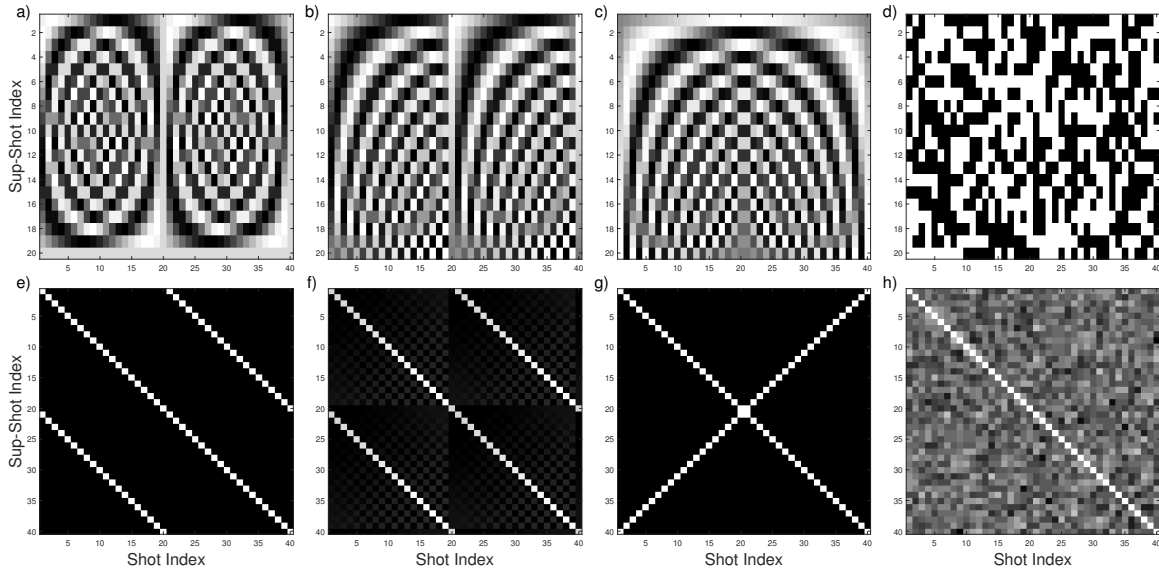

FIG. 14. The amplitude encoding and corresponding crosstalk matrices: columns from left to right are for Hartley, cosine, sine and random polarity bases.

Also, rather than set the iteration times for our tests, we use an abort criterion to control the inversion progress, which is the defined by the relative misfit change within the last two iterations. If the relative change is smaller than one percent, the inversion stops.

The inversion results are shown in Fig 15. The left column are inverted vp and the right column are inverted vs models, from up to down are inverted parameters by conventional FWI, amplitude-encoding FWI using Hartley, cosine, sine and random polarity bases.

When we compare these results, we may notice there exists some minor difference among different cases. But generally, we can also see elastic FWI using amplitude-encoding strategy can also produce comparable inversion result with no obvious crosstalk noise introduced in the final images as in the acoustic cases, which further proves the feasibility of amplitude-encoding strategy for elastic FWI.
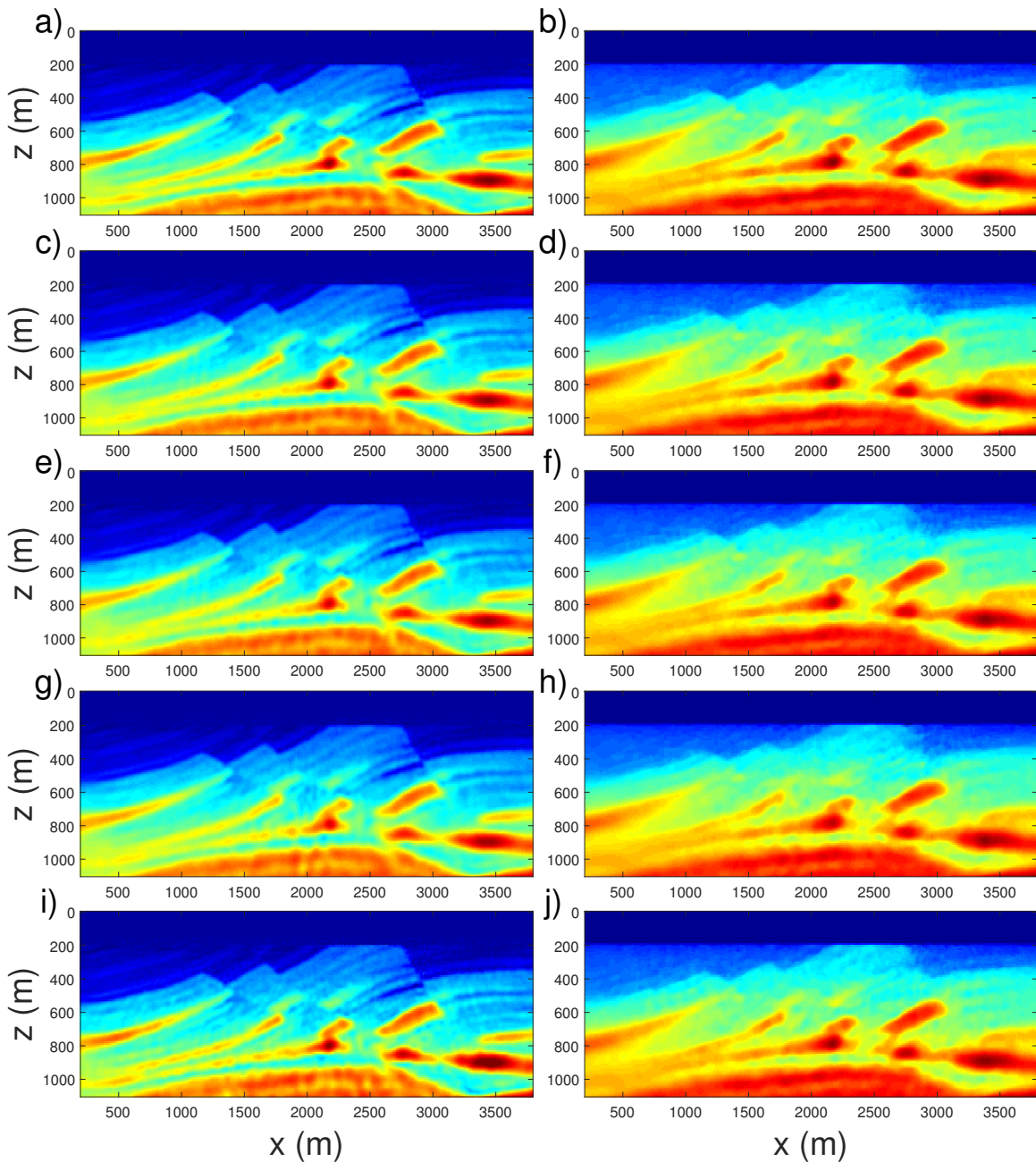
FIG. 15. Inversion results by both conventional and amplitude-encoding FWI: left column is inverted vp, right column is inverted vs; from up to down are inverted parameters by conventional FWI, amplitude-encoding FWI using Hartley, cosine, sine and random polarity bases.

Additionally, vertical vp and vs profiles at 2.2 km of the initial model and inversion results are compared with the true model in Fig 16. The black line is the true model, the dashed red line is the initial model, other thicker lines are the results by amplitude-encoding strategy. The results contain a lot of small details, we can see some fine layers especially in vs model needs further improvement. However, the amplitude-encoding results are still comparable with half reduced calculation effort.
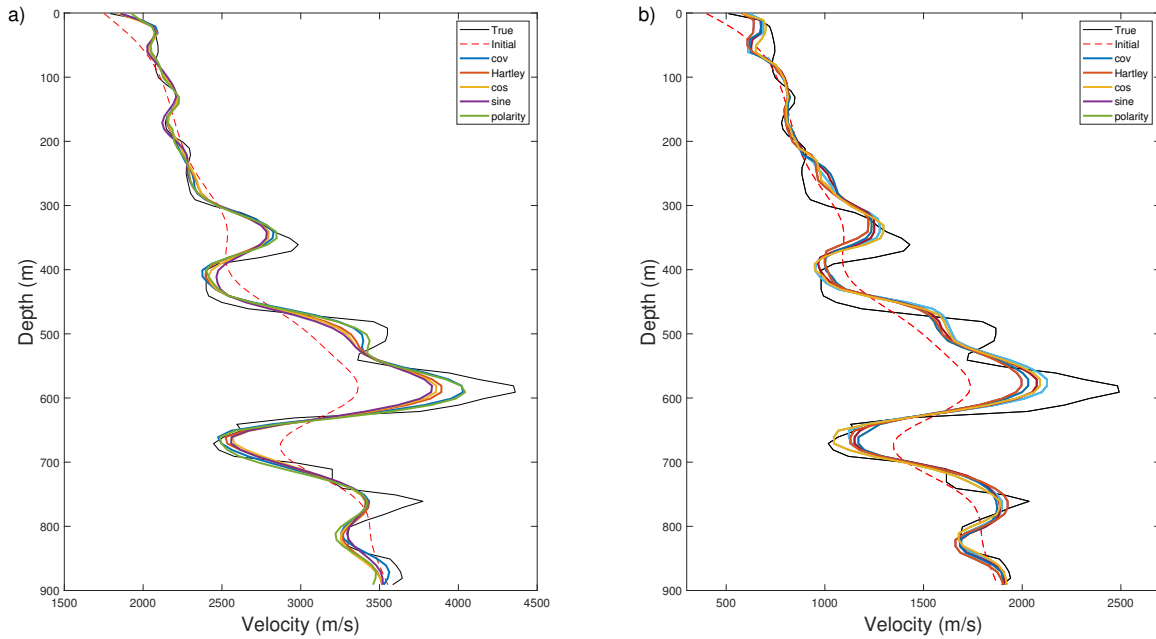
FIG. 16. Depth profiles at distance 2.2 km of the initial model and inversion results are compared with the true model for the Marmousi II model: P-wave velocity (left), S-wave velocity (right).

CONCLUSIONS

In this work, we present the amplitude-encoding acoustic and elastic FWI using different bases as the encoding functions and compare their performance.

In our experiments, we first use Marmousi model to show that amplitude-encoding acoustic FWI using different bases can mitigate the crosstalk noise very well and produce totally comparable inverted models and convergence rate to the conventional case. Then we demonstrate the feasibility of this strategy using a foothill model. What's also worth to notice is that, for conventional acoustic FWI, it requires N_{sig} forward model operations to generate the synthetic acoustic data. While for amplitude-encoding FWI, we can directly simulate N_{sup} super-shots without the blending stage, which also helps improve the calculation efficiency for both forward modelling and inversion process.

In addition, we adopt the dynamic-encoding concept and reduce the number of super-shots during the inversion process to further improve the calculation efficiency, producing almost the same updated velocity models as in the static-encoding cases.

We further apply amplitude-encoding strategy to elastic FWI and prove that this strategy also shows great performance for multi-parameter FWI.

ACKNOWLEDGMENTS

software IFOS2D.

REFERENCES

Bohlen, T., Nil, D., Groos, L., Heider, S., Köhn, D., Kurzmann, A., Schaefer, M., Gassner, L., Metz, T., Thiel, N. et al., 2016, Ifos2d, version 2.0. 3.

Collino, F., and Tsogka, C., 2001, Application of the perfectly matched absorbing layer model to the linear elastodynamic problem in anisotropic heterogeneous media: Geophysics, **66**, No. 1, 294–307.

Dai, W., Fowler, P., and Schuster, G. T., 2012, Multi-source least-squares reverse time migration: Geophysical Prospecting, **60**, No. 4-Simultaneous Source Methods for Seismic Data, 681–695.

Florez, K. A., Mantilla, J. G., and Ramirez, A. B., 2016, Full waveform inversion (fwi) in time for seismic data acquired using a blended geometry, *in* 2016 XXI Symposium on Signal Processing, Images and Artificial Vision (STSIVA), IEEE, 1–5.

Godwin, J., and Sava, P., 2013, A comparison of shot-encoding schemes for wave-equation migration: Geophysical Prospecting, **61**, 391–408.

Hu, J., Wang, H., Fang, Z., Li, T., and Zhang, J., 2016, Efficient amplitude encoding least-squares reverse time migration using cosine basis: Geophysical prospecting, **64**, No. 6, 1483–1497.

Krebs, J. R., Anderson, J. E., Hinkley, D., Neelamani, R., Lee, S., Baumstein, A., and Lacasse, M.-D., 2009, Fast full-wavefield seismic inversion using encoded sources: Geophysics, **74**, No. 6, WCC177–WCC188.

Morton, S. A., and Ober, C. C., 1998, Fastershot-record depth migrations using phase encoding, *in* SEG Technical Program Expanded Abstracts 1998, Society of Exploration Geophysicists, 1131–1134.

Pan, W., 2017, Waveform inversion for estimating subsurface properties: phase-encoding strategies, optimization methods, interparameter tradeoffs quantification and reduction.

Romero, L. A., Ghiglia, D. C., Ober, C. C., and Morton, S. A., 2000, Phase encoding of shot records in prestack migration: Geophysics, **65**, No. 2, 426–436.

Symes, W. W., 2008, Migration velocity analysis and waveform inversion: Geophysical prospecting, **56**, No. 6, 765–790.

Tarantola, A., 1984, Inversion of seismic reflection data in the acoustic approximation: Geophysics, **49**, No. 8, 1259–1266.

Tsitsas, N. L., 2010, On block matrices associated with discrete trigonometric transforms and their use in the theory of wave propagation: Journal of Computational Mathematics, 864–878.

Virieux, J., Asnaashari, A., Brossier, R., Métivier, L., Ribodetti, A., and Zhou, W., 2017, An introduction to full waveform inversion, *in* Encyclopedia of exploration geophysics, Society of Exploration Geophysicists, R1–1.

Yang, P., Gao, J., and Wang, B., 2015, A graphics processing unit implementation of time-domain full-waveform inversion: Geophysics, **80**, No. 3, F31–F39.

Zhan, G., Boonyasiriwat, C., Dai, W., and Schuster, G., 2009, Multi-source waveform inversion with deblurring: Journal of seismic exploration.